This article has been accepted for inclusion in a future issue of this journal. Content is final as presented, with the exception of pagination.

Design and Control of a Novel Bionic Mantis Shrimp Robot

Gang Chen, *Member, IEEE*, Yidong Xu, *Student Member, IEEE*, Chenguang Yang, *Senior Member, IEEE*, Xin Yang, Huosheng Hu, *Life Senior Member, IEEE*, Xinxue Chai, and Donghai Wang

***Abstract*—This article presents the development of a novel bionic robot, which is inspired by agile and fast mantis shrimp in the ocean. The developed bionic mantis shrimp robot has ten rigid-flexible swimming feet (pleopods) for swimming propulsion and a rope-driven spine for its body bending. By studying the motion trajectory of biological mantis shrimp, the kinematic gait planning of the bionic pleopod is completed and the central pattern generator controller of the bionic mantis shrimp robot applicable to the coupled motion of multiple pleopods is proposed. The controller is experimentally verified to effectively simulate the swimming motion of mantis shrimp, which enables the robot to reach a maximum swimming velocity of 0.28 m/s (0.46 body length per second) and a minimum turning radius of 0.36 m.The influence of control parameters on the robot's swimming performance is then investigated. Experiments are conducted to show that the oscillation frequency of the bionic pleopod plays a major positive role in the robot's swimming speed. This article has demonstrated the effectiveness of the proposed mechanism design and motion control method for a bionic mantis shrimp robot and laid the foundation for the further exploration of bionic mantis shrimp robots in rugged seabed environments.**

Manuscript received 18 January 2023; revised 27 March 2023; accepted 4 April 2023. Recommended by Technical Editor D. Chen and Senior Editor W.J. C. Zhang.This work was supported in part by the National Natural Science Foundation of China under Grant 52275037, 51875528, and Grant 41506116, in part by Zhejiang Provincial Natural Science Foundation of China under Grant LY20E050018 and Grant LTY21F030001, in part by the Key Research and Development Project of Zhejiang Province under Grant 2021C04017, and in part by the Science Foundation of Zhejiang Sci-Tech University under Grant 17022183-Y. *(Corresponding authors: Gang Chen; Chenguang Yang.)*

Gang Chen is with the Faculty of Mechanical Engineering and Automation, Zhejiang Sci-Tech University, Hangzhou 310018, China, and also with the School of Computer Science and Electronic Engineering, University of Essex, CO4 3SQ Colchester, U.K. (e-mail: gchen@zstu.edu.cn).

Yidong Xu, Xin Yang, Xinxue Chai, and Donghai Wang are with the Faculty of Mechanical Engineering and Automation, Zhejiang Sci-Tech University, Hangzhou 310018, China. (e-mail: 202130605327@mails.zstu.edu.cn; 201930506060@mails.zstu.edu.cn; chaixx@zstu.edu.cn; donghaiwang@zstu.edu.cn).

Chenguang Yang is with the Bristol Robotics Laboratory, University of the West of England, BS16 1QY Bristol, U.K. (e-mail: cyang@ieee.org).

Huosheng Hu is with the School of Computer Science and Electronic Engineering, University of Essex, CO4 3SQ Colchester, U.K. (e-mail: hhu@essex.ac.uk).

Color versions of one or more figures in this article are available at https://doi.org/10.1109/TMECH.2023.3266778.

Digital Object Identifier 10.1109/TMECH.2023.3266778

***Index Terms*—Bionic robot, central pattern generator (CPG) control, gait planning, mantis shrimp, rigid-flexible pleopod, rope-driven.**

I. Introduction

After a long time of environmental adaptation, the motion mechanism of organisms in nature is more advantageous than that of ordinary propeller propulsion. Marine organisms are capable of both fast swimming and agile maneuverability. As one of the most capable predators in shallow water, mantis shrimp are characterized by powerful forelimbs that produce bullet-like acceleration to deliver devastating blows to their prey targets in tropical and subtropical marine environments. Their swimming speed is extremely fast and can reach to a maximum speed of 30 body lengths per second. Their flat and bendable body structure can reduce fluid resistance and increase their maneuverability in swimming. The pleopods are the main source of thrust for a mantis shrimp. The flexible and multiple pair pleopods reduce drag and generate high propulsive forces.

Some underwater bionic robots, which have high mobility, adaptability, and excellent workability [1], have been developed for real-world applications [2], [3]. Considerable research has also been conducted on mantis shrimp. For instance, Li et al. [4] used a rhombus four-linkage mechanism to stretch the spring to simulate the forelimb of a mantis shrimp. The design effectively stored elastic energy and achieved a performance close to the prechelate motion of mantis shrimp. Steinhardt et al. [5] established a physical model of the impact mechanism of mantis shrimp, simulated the linkage mechanism of the forelimb movement of mantis shrimp, and realized ultrafast movement. Garayev and Murphy [6] measured and analyzed the motion of biological mantis shrimp with a planar particle image velocimeter and found that the phase lag between the pleopods, the motion frequency, and the vortices caused by the pleopods would affect the motion speed or efficiency. Blair et al. [7] studied the vision system of mantis shrimp and developed a six-channel color/near-infrared image sensor that could guide cancer surgery.

Many researchers are attracted by the extraordinary percussion ability [8] and unique visual system of mantis shrimp and have conducted in-depth research. Nevertheless, there are few studies on the movement of pleopods of mantis shrimp. The research on the pleopod movement is only limited to analyzing

This article has been accepted for inclusion in a future issue of this journal. Content is final as presented, with the exception of pagination.

and explaining the influence of their pleopod movement on the overall movement from experimental fluid dynamics. Systematic study on the movement trajectories of multiple pairs of pleopods and their relationship with the overall movement has not been conducted, and the application of biological pleopod movement has not been realized. No researchers have imitated the pleopod motion of mantis shrimp to create a related bionic robot. Therefore, studying the pleopod structure and flexible body structure of biological mantis shrimp and realizing a bionic mantis shrimp robot are of great significance for the movement planning and control of multiple pleopods.

The excellent motion ability of an underwater bionic robot is realized through motion control [9], [10]. To adapt to different underwater environments, many controllers, such as adaptive controller, sliding mode variable structure controller, and neural network controller, have been proposed. These controllers have good adaptability and robustness to the complex underwater environment. However, their feedback process is often very complex, and substantial parameters need to be adjusted. [11]. Central pattern generators (CPGs) are nervous systems found in invertebrates and vertebrates that produce rhythmic neural activity patterns and implement coordinated rhythmic movements [12], [13], [14]. CPG controllers decrease the time delay of the motion control loop, greatly reduce the dimension of the descending control signal, and improve the motion control efficiency of robots. They are widely used in bionic robots [15]. Many motion control models based on CPG, which can realize various motion control modes, such as flight, jumping, walking, and running, have been established [16], [17], [18], [19]. Each CPG system is built for a specific task [20]. Hence, if we want to perform a different task, we need to change the structure of the CPG to meet the movement needs of the robot [21].

This article aims to study the design and CPG motion control of a bionic mantis shrimp robot. The main contributions are as follows.

1) Based on the swimming mode of the mantis shrimp, we developed an agile robot with strong propulsion consisting of ten pleopods and a flexible body. The robot has the following four main advantages.
   a) The bionic mantis shrimp robot is driven by five pairs of pleopods. A balance of velocity and stability can be achieved through adjusting the movement frequency, amplitude, and phase difference of the motion of five pairs of pleopods. In addition, the connection of each pair of pleopods is independent, which is very useful for repairing in case of structural damage underwater.
   b) The turning of the bionic mantis shrimp robot is achieved by bending the flexible torso with a wire rope and the movement of multiple pleopods, which can quickly adjust the turning angle by driving the flexible torso with the wire rope. Furthermore, the multiple pleopods are redundant, which can enable the robot to realize turning even when some of the pleopods fail.
   c) The bionic pleopod is designed with three joints, one of which is an active joint driven by servomotor and the remaining two joints are passive joints, which use the resistance of water to achieve unfolding and folding. When the pleopod moves backward, the three joints are fully expanded to provide maximum propulsion. When the pleopod returns, the passive joints fold to reduce the forward resistance. The design makes full use of the water flow characteristics, simplifies the driving structure, improves the propulsion capacity and reduces the control difficulty.
   d) The overall structure of the bionic mantis shrimp robot refers to the biological mantis shrimp structure and the robot body is flat with a streamlined telson to effectively reduce drag. The pleopod and body of the robot adopt rigid-flexible coupling design to reduce the impact of water on the robot and improve the stability of the robot in underwater motion.
2) We propose a CPG controller for the bionic mantis shrimp robot applicable to the coupled motion of multiple pleopods and verify the effectiveness of the controller through experiments. For this contribution we have done the following work.
   a) The kinematic gait planning of the bionic pleopod was completed by studying the motion mechanism of the biological mantis shrimp and labeling and analyzing its motion trajectory.
   b) The effectiveness of the controller is verified and the effective swimming motion of the robot is realized by analyzing the characteristics of each control parameter of the CPG controller.
   c) To coordinate the CPG control system with the mechanical system of the bionic mantis shrimp robot, we design the topology of the CPG controller, which combines the motion characteristics of the biological mantis shrimp and the mechanical structure of the bionic mantis shrimp robot. The topology is experimentally demonstrated to be very effective for the binoic mantis shrimp robot with coupled motions of multiple pleopods.

This article can provide a new underwater platform for the detection of complex underwater environment. The rest of this article is organized as follows. Section II presents the structure design of the proposed bionic mantis shrimp robot. In Section III, gait planning is proposed for the pleopod swimming of the bionic mantis shrimp robot based on the motion of a real mantis shrimp. Section IV introduces the CPG control method used to control the proposed bionic mantis shrimp robot. Experiments are conducted in Section V to verify the swimming performance of the bionic mantis shrimp robot. Finally, a brief conclusion and future work are given in Section VI.

II. Design of the Bionic Mantis Shrimp Robot

As shown in Fig. 1(a), a mantis shrimp consists of five main parts: head, carapace, walking feet, pleopods, and telson. It uses its walking feet to crawl and relies on the paddling of the pleopods to swim. Based on the physiological structure and movement characteristics of a mantis shrimp, we design a bionic mantis shrimp robot, which consists of four main parts:

This article has been accepted for inclusion in a future issue of this journal. Content is final as presented, with the exception of pagination.

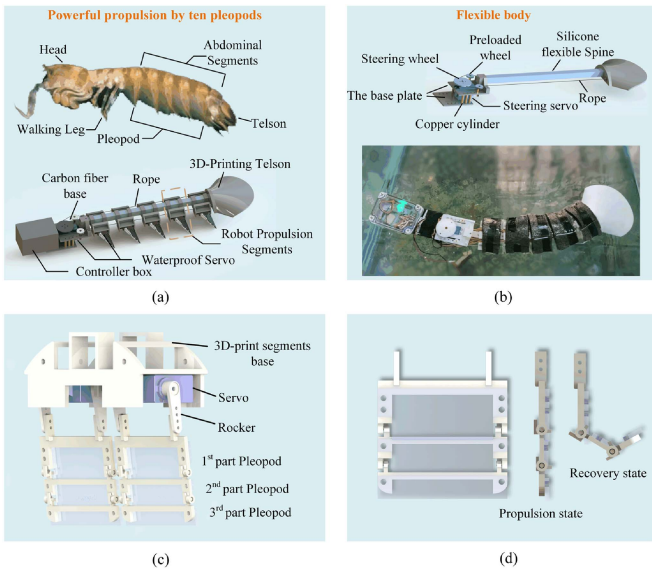

Fig. 1. Mantis shrimp and bionic mantis shrimp robot. (a) Mantis shrimp and robot model. (b) Bionic mantis shrimp robot platform. (c) Robot's propulsion segment. (d) Pleopod and its two working states.

head; flexible body; bionic pleopod; and telson. The head of the robot, i.e., a waterproof box, has a built-in controller and is fixed to a carbon fiber base. The flexible body consists of a wire rope, silicone spine, and five propulsion segments. Due to the small size of some parts, to ensure the assembly accuracy and better durability of the robot, photosensitive resin is selected as the material for three-dimensional (3-D) printing. Compared with the more commonly used polylactic acid polymer material, photosensitive resin has higher accuracy and better toughness. A waterproof servo for pulling the wire rope is located in the carbon fiber base. A propulsion segment consists of a 3-D-printed segment base, two waterproof servos, and a three-joint bionic pleopod. The pleopod is 3-D printed with an elastic silicone film fixed by screws on one side and has two states (propulsion state and recovery state) when it moves forward and backward. The robot's telson is also 3-D printed, attached to the end of the elastic spine to hold the wire rope, and secured with a buoyancy material. The bionic mantis shrimp robot in this article adopts a rigid and flexible coupling design. The elastic deformation of flexible materials when subjected to external forces can well meet the motion requirements of the proposed robot; to a certain extent, it can reduce the interference of water flow on the robot [22]. A rigid structure can make flexible materials produce limited elastic deformation. Meanwhile, the production of rigid structures is more mature, and the production cost is lower, which is very beneficial to our research. The assembled prototype of the bionic mantis shrimp robot is shown in Fig. 1(b).

Fig. 1(c) shows the structure of a single propulsion segment of the bionic mantis shrimp robot with a pair of waterproof servos and two pleopod mechanisms. The waterproof servos drive the pleopod mechanisms in the working plane via a 3-D-printed rocker arm to perform reciprocating rotation movements. Fig. 1(d) depicts the two states of the robot's pleopod: propulsion state and recovery state. In nature, the pleopod of a mantis shrimp also has these two main states when swimming, which provide greater forward propulsion while reducing the forward resistance to the pleopod in recovery. The bionic pleopod consists of a 3-D-printed frame with an elastic silicone film, and the passive joints on the frame are limited so that it can paddle as a biological pleopod without an active actuation.

TABLE I
DESIGN PARAMETERS OF THE ROBOT

Design Parameter	Value (mm)
Prototype robot (length*width*height)	600*65*75
Segment base (length*width*height)	42*78*34
Distance between segment bases	14
Robot pleopod (length*width*height)	45*42*2
Silicone spine (length*width*height)	350*15*15
Controller box (length*width*height)	95*55*65

The bending of the robot is achieved by a steering servo and a rope traction device [23]. The wire rope starts from the steering servo, passes through the propulsion segments one by one, and is finally fixed at the telson. When the steering servo rotates, it can drive the silicone spine to bend. Table I gives the design parameters of the developed robot.

The design size of the bionic mantis shrimp robot in this article is based on the size of a biological mantis shrimp; finally, it is designed on a certain scale. In the structure of the biological mantis shrimp, the pleopod part accounts for about 2/5 of its body length, while that of the robot designed in this article accounts for 1/2 of its length. Thus, the overall ratio is close. Through comparison, the smallest type of waterproof steering gear we can obtain is KM0950MD, whose length $*$ width $*$ height is 25 mm$*$25 mm$*$13 mm. The bionic mantis shrimp robot in this article has five pairs of pleopods, i.e., ten servos are needed to control the pleopod movement, which is an important reference for the overall size of the robot. The pleopod servos are mounted on a 3-D-printed skeleton, so the size of the skeleton is based on the size of the servos. The main factors to be considered for the 3-D-printed skeleton interval are the diameter of the rotating disc of the steering servos and the degree of left and right curvatures of the flexible spine, which are adjusted after many tests and can meet the needs of the current research.

III. KINEMATIC MODELING AND GAIT PLANNING OF THE PLEOPOD

A. Kinematic Modeling of the Pleopod

In accordance with the structural characteristics of the pleopod of the mantis shrimp imitation robot, the coordinate system shown in Fig. 2 is established for the pleopod joint of the robot based on the D–H parameter method. The first joint of the pleopod is the active joint, which is realized through the steering gear movement, while the second and third joints are passive joints,

This article has been accepted for inclusion in a future issue of this journal. Content is final as presented, with the exception of pagination.

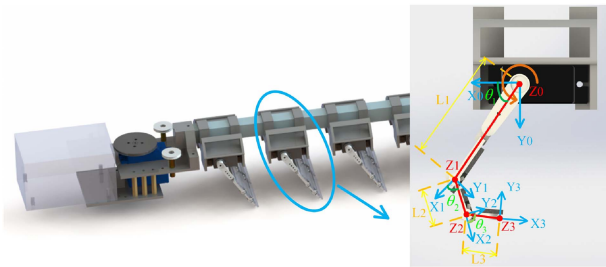

Fig. 2. Coordinate system definition of the bionic pleopod.

TABLE II
D-H PARAMETERS OF THE ROBOT PLEOPOD

i	α_{i-1}	a_{i-1}	d_i	θ_i
1	0	L_1	0	θ_1
2	0	L_2	0	θ_2
3	0	L_3	0	θ_3

which are mainly affected by mechanical limits and water flow. The base of the steering gear is set as the reference coordinate system $X_0Y_0Z_0$, and the coordinate systems $X_1Y_1Z_1$–$X_3Y_3Z_3$ of the first joint to the third joint are established successively. At this time, all joints are in a plane and are rotary joints. A DH parameter table of the bionic pleopod can be established according to the coordinate system, as given in Table II. In the table L_1, L_2, and L_3 refer to the lengths of the joints, and Θ_i is the rotation angle between two joints.

According to the D–H parameter table, the joint homogeneous transformation matrix is

$$ {}^{i-1}_{\ \ i}T = \begin{bmatrix} c\theta_i & -s\theta_i & 0 & L_i \cdot c\theta_i \\ s\theta_i & c\theta_i & 0 & L_i \cdot s\theta_i \\ 0 & 0 & 1 & 0 \\ 0 & 0 & 0 & 1 \end{bmatrix} \tag{1} $$

$c\theta$ and $s\theta$ are short for $\cos\theta$ and $\sin\theta$, respectively. The coordinates of each joint in the pleopod joint coordinate system can be calculated according to the servo motion angle. Therefore, the forward kinematics of the bionic pleopod is as follows:

$$ \begin{aligned} {}^0_3T &= {}^0_1T\,{}^1_2T\,{}^2_3T \\ &= \begin{bmatrix} c_{123} & -s_{123} & 0 & L_3 \cdot c_{123} + L_2 \cdot c_{12} + L_1 \cdot c_1 \\ s_{123} & c_{123} & 0 & L_3 \cdot s_{123} + L_2 \cdot s_{12} + L_1 \cdot s_1 \\ 0 & 0 & 1 & 0 \\ 0 & 0 & 0 & 1 \end{bmatrix} \end{aligned} \tag{2} $$

$$ \begin{aligned} c_1 &= \cos\theta_1; s_1 = \sin\theta_1 \\ c_{12} &= \cos(\theta_1 + \theta_2); s_{12} = \sin(\theta_1 + \theta_2) \\ c_{123} &= \cos(\theta_1 + \theta_2 + \theta_3); s_{123} = \sin(\theta_1 + \theta_2 + \theta_3). \end{aligned} $$

Based on the formula, the trajectory of the end of the pleopod can be calculated according to the motion angles of each joint.

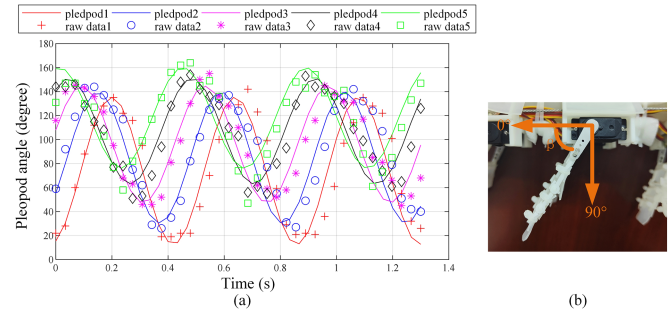

Fig. 3. Swimming trajectories of mantis shrimp. (a) Sampling results from a swimming video of mantis shrimp and their fitting trajectory curve. (b) Paddling angle definition of the pleopod.

TABLE III
PARAMETERS OF THE SWIMMING TRAJECTORIES OF PLEOPODS

Index of Pleopod	Parameters		
i	a	b	c
1	74	-61	-6
2	85	45	31
3	96	-7	48
4	107	22	38
5	118	35	23

B. Swimming Gait Planning of the Robot

For a bionic mantis shrimp robot, the swimming gait planning of its bionic pleopod plays a key role in achieving its bionic swimming capabilities. From the video data of about 30 s (30 fps), the swing angle of the pleopod is manually marked at an interval of 66.7 ms (15 fps). The pleopod motion is analyzed and modeled to obtain its kinematic equations. The paddling angle of the pleopod is defined, as shown in Fig. 3(b). Its raw sampling data are presented in Fig. 3(a), where x and y represent the time and paddling angle of the pleopod.

Through using the cftool toolbox in MATLAB [24] to fit the sampled points, the swimming trajectories of pleopods can be obtained, where the R-square between each fitted curve and its original data point is above 0.9. The fitting function is as follows:

$$ \beta_i(t) = a_i + b_i \times \cos(\omega t) + c_i \times \sin(\omega t), 1 \le i \le 5 \tag{3} $$

where $\beta_i(t)$ is the swimming angle; ω is the frequency factor; i is the index of the pleopod; a_i, b_i, and c_i are the magnitude coefficients of the constant, sine, and cosine terms of the fitting function [25]. The gait planning parameters for each bionic pleopod swimming gait are given in Table III, which mainly change the amplitude of the oscillation of each pair of pleopods and the initial and ending positions of the oscillation. When the biological mantis shrimp swims, the swing angle of each pair of pleopods is inconsistent. Hence, each pair of pleopods needs a set of parameters to control the corresponding motion angle. In the fitting function of each pair of pleopods, five pairs of pleopods share a common swing frequency ω. Although the

This article has been accepted for inclusion in a future issue of this journal. Content is final as presented, with the exception of pagination.

angle of the swing is different at each moment, the motion state of the five groups of pleopods is related.

As shown in Fig. 3(a), the fitting trajectories of the five pairs of pleopods represented by curves 1–5 can be used as a basis swimming gait planning result for the bionic mantis shrimp robot.

IV. CPG-Based Locomotion Control

Based on the swimming trajectories of pleopods, we propose a CPG controller for the rhythmic swimming of our bionic mantis shrimp robot. The CPG oscillator model for our robot can be described as follows:

$$\dot{\theta}_i = \omega_i + \sum_j r_{1j} w_{ij} \sin\left(\theta_j - \theta_i - \varphi_{ij}\right) \tag{4}$$

$$\ddot{r}_{1i} = \alpha_i \left(\frac{\alpha_i}{4}\left(R_{1i} - r_{1i}\right) - \dot{r}_{1i}\right) \tag{5}$$

$$\ddot{r}_{2i} = \alpha_i \left(\frac{\alpha_i}{4}\left(R_{2i} - r_{2i}\right) - \dot{r}_{2i}\right) \tag{6}$$

$$\ddot{x}_i = \alpha_i \left(\frac{\alpha_i}{4}\left(X_i - x_i\right) - \dot{x}_i\right) \tag{7}$$

$$\beta_i = x_i + r_{1i}\cos\theta + r_{2i}\sin\theta \tag{8}$$

where ω_i is the desired frequency of the oscillator. x_i, r_{2i}, and r_{1i} are the amplitude state variables of the output deviation term, sine term, and cosine term in the oscillator i. α_i refers to constant positive gains. w_{ij} and φ_{ij} are the coupling weights and phase biases, respectively, which determine how oscillator j influences oscillator i. R_{1i}, R_{2i}, and X_i are the parameters of the controller representing the desired amplitude of each corresponding output term of the oscillator. β_i represents the final output angle of each oscillator.

The oscillator output model can easily fit the motion characteristics of the bionic mantis shrimp robot according to the gait planning parameters. In addition, the model inherits the characteristics of the Ijspeert oscillator, which can directly adjust the frequency and phase difference of several amplitude parameters [18] and can quickly return to steady-state oscillation when the oscillator is affected by transient interference. Fig. 4 shows the effect of the results of the oscillator parameters on the output of a single CPG oscillator. The number of cycles of the CPG operation is used as the horizontal axis, and the output angle of the oscillator is used as the vertical axis. The dotted line represents the node where the parameter changes, and the blue curve is the actual output of the oscillator.

The CPG model in this article has a total of six oscillators, among which five CPG oscillators control the movement of the five pairs of pleopods, and one CPG oscillator controls the turning of the body. Under normal conditions, the output of the CPG oscillators for the five pairs of pleopods is periodic, while the output of the CPG oscillator controlling the body steering is constant, not periodic. Fig. 4(a) shows that when the coefficient of other output items is 0, the oscillator output can be made to constant by adjusting the coefficient of the deviation item of the output to be constant, which indicates the effectiveness of the CPG controller on the robot turning control signal. Fig. 4(b) and

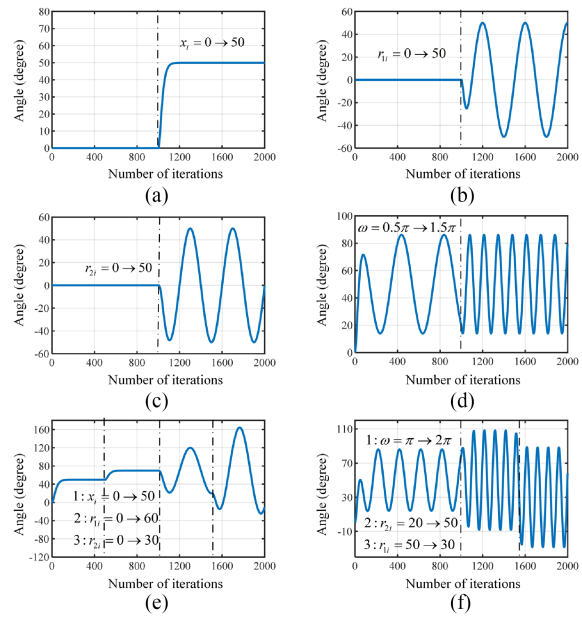

Fig. 4. Effect of CPG parameters on single CPG output. (a) Effect of x_i on the CPG output. (b) Effect of r_{1i} on the CPG output. (c) Effect of r_{2i} on the CPG output. (d) Effect of ω on the CPG output. (e) Effect of x_i, r_{1i}, and r_{2i} on the CPG output. (f) Effect of ω, r_{2i}, and r_{1i} on the CPG output.

(c) shows that when the coefficients of other output terms are 0, adjusting the coefficients of the sine or cosine terms of the output to be constant can make the oscillator output a trigonometric function of the corresponding amplitude. This shows the effectiveness of the CPG controller output on the robot's pleopod control signal. Fig. 4(d) demonstrates that the output frequency of the oscillator can be changed correspondingly by modifying the expected frequency of the oscillator. Fig. 4(e) and (f) show that appropriate changes to multiple parameters of the oscillator can achieve dynamic adjustment of the output without affecting the effectiveness of the oscillator output.

These results indicate that the output of a CPG oscillator can be configured to match the gait planning of the robot, thus implementing the motion of the bionic pleopod. The frequency of the CPG oscillator can also be varied by adjusting the desired frequency parameter, which can be used to adjust the motion frequency of the bionic pleopod.

A single CPG oscillator is typically used to generate rhythmic control signals for a single joint. The bionic mantis shrimp robot has ten independently controllable bionic pleopods and a rope-driven-based flexible spine. Based on these characteristics, a CPG network model for the bionic mantis shrimp robot should be constructed, which can output multiple control signals through the configuration of coupling parameters for agile swimming of the robot.

Fig. 5(a) illustrates the topology of the CPG network consisting of six mutually coupled oscillators. The topology combines the locomotion characteristics of multiple pleopods in the biological mantis shrimp with the mechanical structure of the bionic mantis shrimp robot. CPG-1–CPG-5 is used to configure

This article has been accepted for inclusion in a future issue of this journal. Content is final as presented, with the exception of pagination.

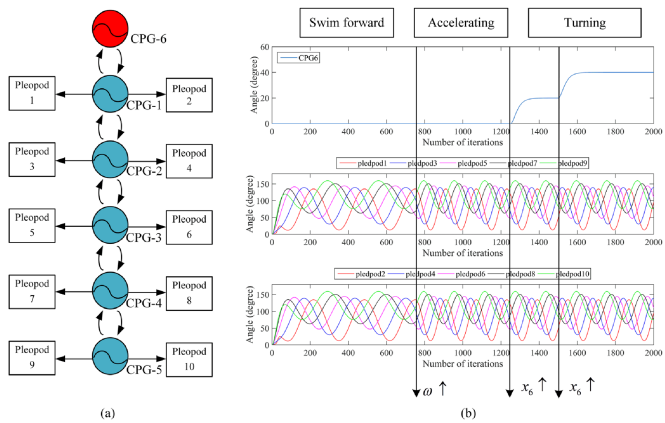

Fig. 5. CPG network and its outputs. (a) CPG network used for robot control. (b) Outputs of CPG-6 and pleopods 1–10 in different locomotion status.

the reference output angles of the five pairs of bionic pleopods, whose parameters are determined according to the values in Table III. CPG-6 is used to configure the output angle of the steering servo. It can be adopted for the bionic mantis shrimp robot after a reasonable configuration of parameters and can achieve the straight swimming and turning motion mode. Fig. 5(b) shows the output of the CPG-6 controller.

In the straight motion, the output of CPG-6 is always zero, and the left and right pleopods are output at the same angle based on the same CPG, producing a balanced and forward propulsion force. In the turning motion, the output of CPG-6 is not zero and drives the central servo to pull the flexible spine to bend. At this time, each bionic pleopod maintains its original paddling state to generate torque for turning motion.

In the CPG network, phase differences in the pleopod motion are achieved by parameter configuration of the output item. Test results show that the desired bionic pleopod gait is obtained when φ is 0. In addition, a relationship exists between the value of the weighted coupling parameter φ and the desired frequency of oscillator ω. Its ratio is defined as the lagging parameter L

$$L = \frac{\varphi}{\omega}. \tag{9}$$

Varying the value of the coupling weights φ_{ij} according to the desired frequency ω creates an additional phase difference between adjacent oscillators. The adjustment of the lag factor reflects the interval that generates the same cycle ratio between adjacent CPGs in a motion cycle of different time lengths. Fig. 6 shows the effect of the weighted coupling parameter on the output of the CPG oscillators. The outputs of CPG-1–CPG-5 are shown in Fig. 6(a) and (b) when the ratio L is 0 and 0.2. The output of CPG-1 oscillator is plotted in Fig. 6(c) with L values of 0, 0.1, 0.2, and 0.4. When L is from 0 to 0.2, the output of the CPG network model can maintain the basic form of the gait planning, and the phase difference between adjacent CPG oscillators increases with L.

When L continues to increase to over 0.2, CPG-4 coincides with the output of the next oscillation cycle. At this time, the output of the CPG network model is no longer consistent with

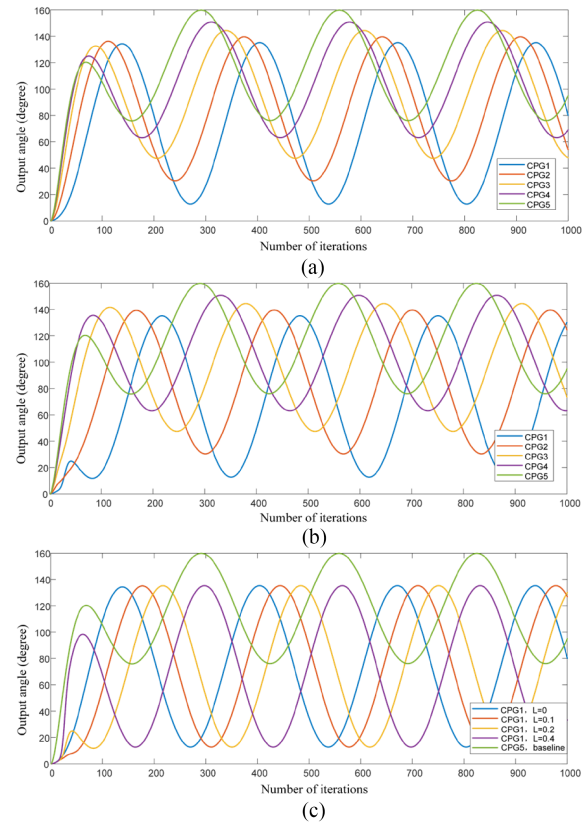

Fig. 6. Effect of L on the output of the CPG network. (a) CPG-1–CPG-5 outputs when $L = 0$. (b) CPG-1–CPG-5 outputs when $L = 0.2$. (c) CPG-1 output when $L = 00.10.20.4$; CPG 5 is the baseline.

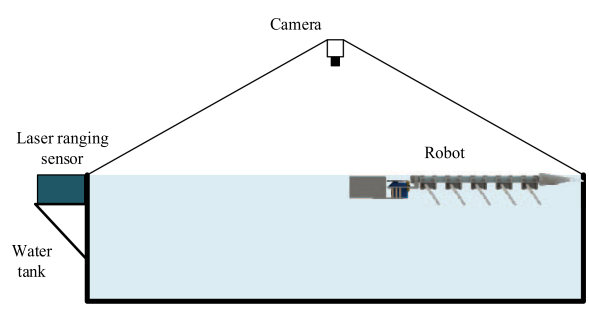

Fig. 7. Experimental platform and equipment.

the gait planning result. A wrong motion state of pleopods may be generated, resulting in the collision of front and rear bionic pleopods.

V. Experiments

An experimental platform is built for robot swimming experiments to verify the effectiveness of the proposed robot structure, gait planning, and CPG controller. Fig. 7 shows the water tank and sensors used for the experiment. The size of the water tank is 2.0 m in length, 1.0 m in width, and 1.0 m in height. In the experimental part, the robot's movement is recorded mainly through a camera and a laser rangefinder. The camera is fixed on the top of the pool, which is used to photograph the robot's

This article has been accepted for inclusion in a future issue of this journal. Content is final as presented, with the exception of pagination.

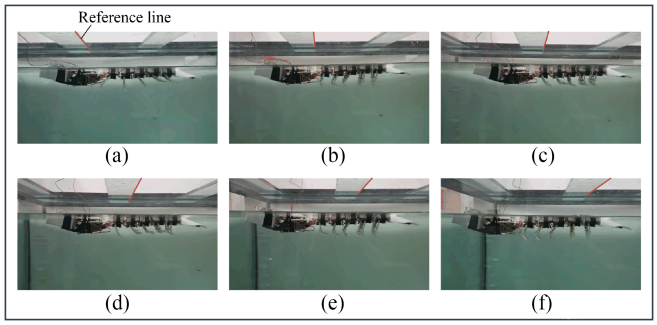

Fig. 8. Moving image sequence.

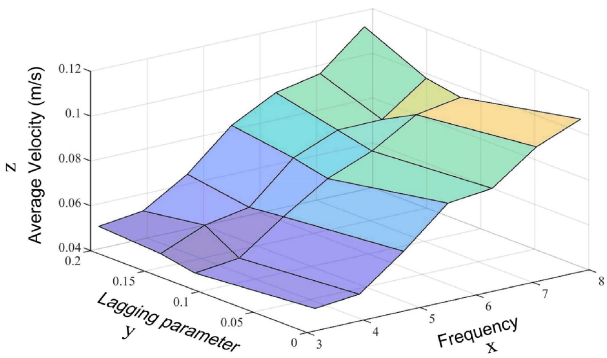

Fig. 9. Effect of CPG parameter on swimming speed.

motion process and obtain the motion position by processing the robot's motion image sequence. The laser rangefinder is installed on one side of the pool and is used to record the distance change of the robot when it goes straight. The motion state of the robot can be obtained after derivation and average calculation of the data.

A. Forward Straight Swimming With Different CPG Parameters

As the swimming speed is a core indicator, this experiment aims to investigate the effect of the robot's CPG parameters on its swimming speed. In the experiment, the steering servo of our bionic mantis-like shrimp robot does not rotate, remaining in its initial position. The robot relies on the thrust generated by the bionic pleopod to achieve forward swimming. The laser ranging sensor is used to measure the robot's motion position and calculate the average speed of the robot in one swimming cycle from one end of the water tank to the other end.

Fig. 8 is the motion diagram of experiment A, which records the robot's straight motion within 5 s. From the movement of five pairs of pleopods in the figure, the movement frequency and phase difference of pleopods can be flexibly controlled by adjusting CPG parameters.

Fig. 9 is shows the experimental results, where Z-axis represents the measured average speed of the robot, X-axis represents the desired frequency of the oscillator, and Y-axis is the lagging parameter L. Twenty-eight sets of experiments are completed, each of which is repeated three times to avoid the effect of chance. The average value is regarded as the result of each set of experiments.

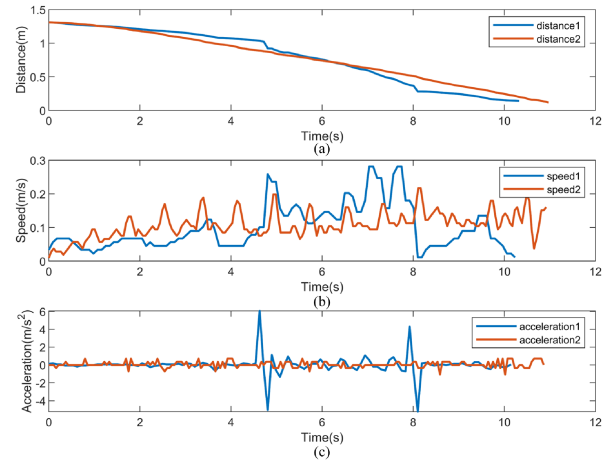

Fig. 10. Position, velocity, and acceleration of the robot when the lagging parameter L is 0 (blue) and 0.2 (red).

The previous sections showed that changing the lagging parameter produces an additional phase difference between neighboring CPG oscillators. Here, the experimental results present that when the oscillation frequency is increased, the average speed of the robot's movement is also increased. However, the effect of the lagging parameter on the speed is not obvious, although the overall trend can be observed as the speed tends to decrease and then increase when increasing from 0.

In the experiment, the maximum average speed of the robot in the water tank is measured to be approximately 0.12 m/s. The maximum speed that could be achieved after sufficient average acceleration is approximately 0.28 m/s (0.46 body length per second).

B. Swimming Experiments With Variable Lagging Parameters

In this experiment, the experimental environment is set up in the same way as in experiment A. The content of experiment B is the straight swimming of the robot under different hysteresis parameters. In this article, the change in hysteresis parameters is the phase difference of the motion of the five pairs of pleopods. In the experiment, except for different hysteresis parameters, the other settings are the same. The hysteresis parameters in experiments 1 and 2 are 0 and 0.2, respectively, and the inherent frequencies of robot motion are both 2.5 π. The distance change of the robot from far to near is measured using the laser rangefinder. Then, we filter the mean value of the data and compute the derivatives to obtain the changes in the distance, speed, and acceleration of the robot during its movement. Fig. 10 shows the experimental results. Specifically, the results for relative distance, velocity, and acceleration in experiments 1 and 2 are given in Fig. 10(a)–(c), respectively.

From the experimental results, the robot achieves a maximum instantaneous speed of 0.28 m/s and an average speed of 0.1 m/s with the lagging parameter set to 0. The acceleration data in

This article has been accepted for inclusion in a future issue of this journal. Content is final as presented, with the exception of pagination.

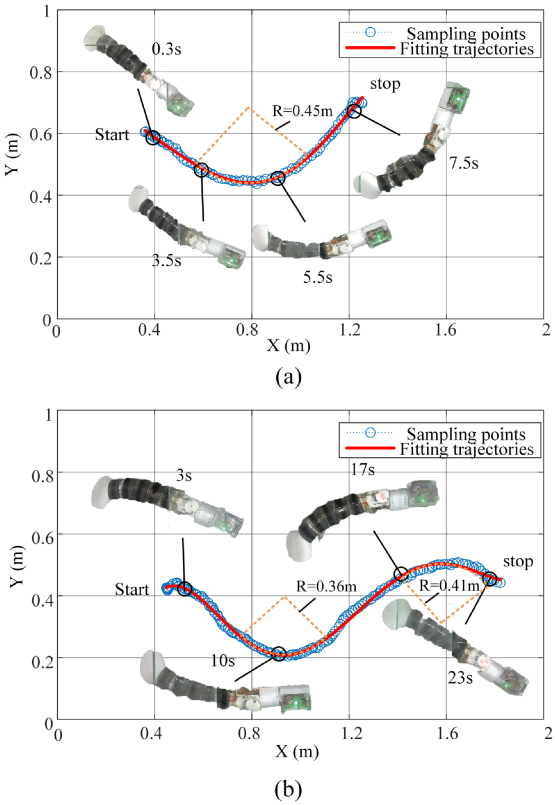

Fig. 11. Turning motion experiments of the robot. (a) One turning experiment. (b) Continuous turning experiment.

Fig. 10(c) show that the robot has two sudden accelerations in the middle of the motion. The speculation is that when the phase parameter is 0, the phase difference between the front and rear pleopods is small, and the motion is more intensive, which can generate more propulsion and impact the motion stationarity. When the lagging parameter is 0.2, the phase difference between the front and rear pleopods is large. Thus, the robot's velocity exhibits a periodic variation and is smoother, i.e., speed2 in Fig. 10(b).

C. Forward Swimming and Turning Locomotion

In this experiment, the robot relies on the bionic pleopod to generate thrust and is adjusted by the steering servo for turning movements. The CPG-6 parameters in the CPG network are adjusted, and the robot completes a continuous series of swim motions in the water tank with a camera for recording the robot's movements.

Fig. 11(a) shows the turning motion of our bionic mantis shrimp robot in the water tank. It requires 7.8 s to travel 1.02 m distance; therefore, its average speed is 0.14 m/s. Its turning radius is about 0.45 m. Fig. 11(b) depicts the two turning motions of the robot. The whole movement process takes 23 s, the total distance is 1.52 m, and the average speed is 0.06 m/s. The first turning radius is 0.36 m, and the second turn radius is 0.41 m.

The experimental results indicate that our bionic mantis shrimp robot has good turning capability in water and sufficient potential to be used for complex underwater navigation tasks. During the experiments, the robot rolls sideways because of the excessive body lateralization when the robot conducts high maneuver turning, proposing a challenge for future research on attitude control of bionic mantis shrimp robots.

Based on the experimental results above, the following findings can be obtained.

1) Accelerating the swing frequency of the bionic pleopod can effectively improve the robot's motion speed. In the experiment, the maximum frequency is 3 π, and the maximum average speed is 0.12 m/s.
2) Varying the lagging parameter in CPG, i.e., changing the phase difference in the motion of the pleopod pairs, exerts a minimal effect on the average robot speed theoretically. However, in practice, the lagging parameters could affect the instantaneous speed and posture of the robot. When the lagging parameter is small, the robot exhibits faster instantaneous velocities and more unstable posture with a maximum instantaneous velocity of 0.28 m/s (0.46 BLS/s). However, the opposite results are observed when the phase difference is increased. This result demonstrates that the bionic mantis shrimp robot can operate in both burst and smooth swimming states, presenting the potential bionic locomotor capabilities of the robot.

VI. Conclusion and Future Work

Inspired by nature, a bionic mantis shrimp robot with bionic pleopods and rope-driven spine is developed in this article. The overall design of the robot not only imitates the shape of the mantis shrimp, but also the form of its movement. The bionic pleopod proposed in this article is designed on the basis of the pleopod movement of mantis shrimp. The bionic pleopod makes full use of the characteristics of water flow. It expands during pushing and folds during return journey and can realize three-joint movement with only one servo, forming an active–passive coupling pleopod structure. To implement flexible turning of the robot, bionic spine and joints are designed. The turning movement of the robot is driven by rope. Only one servo is needed to realize turning movement, creating a flexible body structure like that of mantis shrimp. The robot's bionic pleopod and body parts are designed with rigid-flexible coupling to reduce the impact of the water on the robot and improve the stability of the robot's underwater movement.

In addition, we studied the swimming gait planning method of the robot based on the motion characteristics of the biological mantis shrimp and also proposed a robot CPG controller applicable to multiple pleopod motion by combining the mechanical structure of the bionic mantis shrimp robot and the motion characteristics of the biological mantis shrimp. The characterization of the CPG controller is completed and the effects of different control parameters on the swimming velocity of the robot are studied. Experiments verify that the design of the bionic pleopod can provide sufficient propulsion for the robot to move forward, and the rope-driven elastic spine can effectively realize the flexible turning of the robot. The results are given to show that the CPG-based robot motion control system can control the

This article has been accepted for inclusion in a future issue of this journal. Content is final as presented, with the exception of pagination.

bionic mantis shrimp robot to move straight and turn. With two model parameters, the robot can be adjusted for straight and turning movements, as well as acceleration and deceleration. When the movement frequency of the bionic pleopod is greater than 2.5π, structural damage of the robot will occur.

In the future, we will focus on how to realize autonomous movement of the bionic mantis shrimp robot in a narrow underwater environment to complete the detection task in this environment. The main idea is as follows: We will optimize the structure [26], shape, and hardware system design of the robot to improve its six-degree-of-freedom motion ability in 3-D space and higher underwater motion speed. Then, the inertial measurement unit (IMU), camera, depth sensor, and other information acquisition devices will be increased to achieve more accurate closed-loop motion control of the robot through the analysis of environmental information and the feedback adjustment of its own posture. Finally, the practical application ability of the bionic mantis shrimp imitation robot in a cramped underwater environment will be improved. The durability and reliability of each component will be further considered and enhanced by the use of carbon fiber and embedded high-strength materials, thus laying the foundation for practical applications in confined underwater environments.

References

[1] G. Chen, Z. Zhao, Z. Wang, J. Tu, and H. Hu, "Swimming modeling and performance optimization of a fish-inspired underwater vehicle (FIUV)," *Ocean Eng.*, vol. 271, 2023, Art. no. 113748.

[2] P. J. Zhou et al., "Overview of progress in development of the bionic underwater propulsion system," *J. Biomimetics, Biomater. Biomed. Eng.*, vol. 32, pp. 9–19, 2017.

[3] J. Yu, M. Wang, H. Dong, Y. Zhang, and Z. Wu, "Motion control and motion coordination of bionic robotic fish: A review," *J. Bionic Eng.*, vol. 15, no. 4, pp. 579–598, 2018.

[4] X. Li et al., "Mantis shrimp-inspired underwater striking device generates cavitation," *J. Bionic Eng.*, vol. 19, no. 6, pp. 1758–1770, 2022.

[5] E. Steinhardt et al., "A physical model of mantis shrimp for exploring the dynamics of ultrafast systems," *Proc. Nat. Acad. Sci.*, vol. 118, no. 33, pp. 1–11, 2021.

[6] K. Garayev and D. W. Murphy, "Metachronal swimming of mantis shrimp: Kinematics and interpleopod vortex interactions," *Integrative Comp. Biol.*, vol. 61, no. 5, pp. 1631–1643, 2021.

[7] S. Blair et al., "Hexachromatic bioinspired camera for image-guided cancer surgery," *Sci. Transl. Med.*, vol. 13, no. 592, pp. 1–12, 2021.

[8] M. S. Devries, E. A. Murphy, and S. N. Patek, "Strike mechanics of an ambush predator: The spearing mantis shrimp," *J. Exp. Biol.*, vol. 215, no. Pt 24, pp. 4374–4384, 2012.

[9] G. Chen, X. Yang, Y. Xu, Y. Lu, and H. Huosheng, "Neural network-based motion modeling and control of water-actuated soft robotic fish," *Smart Mater. Struct.*, vol. 32, 2023, Art. no. 015004.

[10] G. Chen, Y. Lu, X. Yang, and H. Hu, "Reinforcement learning control for the swimming motions of a beaver-like, single-legged robot based on biological inspiration," *Robot. Auton. Syst.*, vol. 154, 2022, Art. no. 104116.

[11] S. G. Tzafestas, "Mobile robot control and navigation: A global overview," *J. Intell. Robot. Syst.*, vol. 91, no. 1, pp. 35–58, 2018.

[12] A. J. Ijspeert, "Central pattern generators for locomotion control in animals and robots: A review," *Neural Netw.*, vol. 21, no. 4, pp. 642–653, 2008.

[13] S. Grillner, "Neurobiological bases of rhythmic motor acts in vertebrates," *Science*, vol. 228, no. 4696, pp. 143–149, 1985.

[14] U. S. Larry and M. Jordan, "The brain and spinal cord networks controlling locomotion," *CNS Disord., Therapeutics*, pp. 215–233, 2014.

[15] J. Yu, M. Tan, J. Chen, and J. Zhang, "A survey on CPG-inspired control models and system implementation," *IEEE Trans. Neural Netw. Learn. Syst.*, vol. 25, no. 3, pp. 441–456, Mar. 2014.

[16] F. Xie, Y. Zhong, R. Du, and Z. Li, "Central pattern generator (CPG) control of a biomimetic robot fish for multimodal swimming," *J. Bionic Eng.*, vol. 16, no. 2, pp. 222–234, 2019.

[17] H. Rostro-Gonzalez et al., "A CPG system based on spiking neurons for hexapod robot locomotion," *Neurocomputing*, vol. 170, pp. 47–54, 2015.

[18] A. J. Ijspeert, A. Crespi, D. Ryczko, and J. M. Cabelguen, "From swimming to walking with a salamander robot driven by a spinal cord model," *Science*, vol. 315, no. 5817, pp. 1416–1420, 2007.

[19] A. Sprowitz, A. Tuleu, M. Vespignani, M. Ajallooeian, E. Badri, and A. J. Ijspeert, "Towards dynamic trot gait locomotion: Design, control, and experiments with cheetah-cub, a compliant quadruped robot," *Int. J. Robot. Res.*, vol. 32, no. 8, pp. 933–951, Jul. 2013.

[20] A. A. Saputra, N. Takesue, K. Wada, A. J. Ijspeert, and N. Kubota, "AQuRo: A cat-like adaptive quadruped robot with novel bio-inspired capabilities," *Front. Robot. AI*, vol. 8, 2021, Art. no. 562524.

[21] A. Crespi, D. Lachat, A. Pasquier, and A. J. Ijspeert, "Controlling swimming and crawling in a fish robot using a central pattern generator," *Auton. Robots*, vol. 25, pp. 3–13, 2008.

[22] A. Chen, R. Yin, L. Cao, C. Yuan, H. K. Ding, and W. J. Zhang, "Soft robotics: Definition and research issues," in *Proc. IEEE 24th Int. Conf. Mechatronics Mach. Vis. Pract.*, 2017, pp. 366–370.

[23] Y. Zhong, Z. Li, and R. Du, "A novel robot fish with wire-driven active body and compliant tail," *IEEE/ASME Trans. Mechatronics*, vol. 22, no. 4, pp. 1633–1643, Aug. 2017, doi: 10.1109/TMECH.2017.2712820.

[24] Y. Zhang, C. Ding, J. Wang, and J. Cao, "High-energy orbit sliding mode control for nonlinear," *Nonlinear Dyn.*, vol. 105, pp. 191–211, 2021.

[25] J. L. Lim and M. E. Demont, "Kinematics, hydrodynamics and force production of pleopods suggest jet-assisted walking in the American lobster (Homarus americanus)," *J. Exp. Biol.*, vol. 212, no. 17, pp. 2731–2745, 2009.

[26] L. Cao, A. T. Dolovich, A. L. Schwab, J. L. Herder, and W. C. Zhang, "Toward a unified design approach for both compliant mechanisms and rigid-body mechanisms: Module optimization," *J. Mech. Des.*, vol. 137, no. 12, pp. 1–10, 2015.

Gang Chen (Member, IEEE) received the Ph.D. degree in mechatronic engineering from the State Key Laboratory of Fluid Power and Mechatronic Systems, Zhejiang University, Hangzhou, China, in 2014.

He is currently a Professor with the Faculty of Mechanical Engineering and Automation, Zhejiang Sci-Tech University, Hangzhou, China, specializing in intelligent control of bionic robots.

Yidong Xu (Student Member, IEEE) received the Bachelor's degree in engineering from Ningbo University of Technology, Ningbo, China, in 2021. He is currently working toward the Master degree with Zhejiang Sci-Tech University, Hangzhou, China.

His main research direction is underwater bionic robots.

Chenguang Yang (Senior Member, IEEE) received the Ph.D. degree in control engineering from the National University of Singapore, Singapore, in 2010.

He took the postdoctoral training in human robotics from the Imperial College London, London, U.K. His research interest lies in human robot interaction and intelligent system design.

Dr. Yang was the recipient of U.K. EPSRC UKRI Innovation Fellowship and individual EU Marie Curie International Incoming Fellowship. As the lead author, he was also the recipient of IEEE Transactions on Robotics Best Paper Award in 2012 and IEEE Transactions on Neural Networks and Learning Systems Outstanding Paper Award in 2022. He is the Co-Chair of IEEE Technical Committee on Collaborative Automation for Flexible Manufacturing and the Co-Chair of IEEE Technical Committee on Bio-mechatronics and Biorobotics Systems.

This article has been accepted for inclusion in a future issue of this journal. Content is final as presented, with the exception of pagination.

Xin Yang received the Bachelor's degree in engineering from China University of Mining and Technology, Beijing, China, in 2019. He is currently working toward the Master degree with Zhejiang Sci-Tech University, Hangzhou, China.

His main research direction is underwater soft robots and underwater bionic robots.

Huosheng Hu (Life Senior Member, IEEE) received the M.Sc. degree in industrial automation from Central South University, Changsha, China, in 1982, and the Ph.D. degree in robotics from the University of Oxford, Oxford, U.K., in 1993.

He is currently a Professor with the School of Computer Science and Electronic Engineering, University of Essex, Colchester, U.K., where he is leading the Robotics Research Group. He has authored or coauthored more than 420 articles. His current research interests include robotics, human–robot interaction, embedded systems, mechatronics, and pervasive computing.

Dr. Hu is a founding member of the IEEE Robotics and Automation Society Technical Committee on Networked Robots, a fellow of the Institution of Engineering and Technology, and a Senior Member of the Association for Computing Machinery. He is currently an Editor-in-Chief for *International Journal of Automation and Computing* and the *Online Robotics Journal* and an Executive Editor of the *International Journal of Mechatronics and Automation*.

Xinxue Chai received the B.S. and Ph.D. degrees in mechanical engineering from Zhejiang Sci-Tech University, Hangzhou, China, in 2011 and the2017, respectively.

Since 2017, she has been a Lecturer with the Faculty of Mechanical Engineering and Automation, Zhejiang Sci-Tech University, Hangzhou, China.She is an Associate Professor. Her research interest includes mechanism theory using geometric algebra.

Donghai Wang received the B.Eng. and Ph.D. degrees in mechatronics from Zhejiang University, Hangzhou, China, in 2010 and 2016, respectively.

He was a Visiting Scholar with the Georgia Institute of Technology, Atlanta, GA, USA, from 2013 to 2015. He was an Associate Professor with the Faculty of Mechanical Engineering and Automation, Zhejiang Sci-Tech University, Hangzhou, China. His current research interests include robotics and mechatronics.